ARCHIVIO ISTITUZIONALE
DELLA RICERCA

Alma Mater Studiorum Università di Bologna
Archivio istituzionale della ricerca

Multifunctional nanoassemblies target bacterial lipopolysaccharides for enhanced antimicrobial DNA delivery

This is the submitted version (pre peer-review, preprint) of the following publication:

Published Version:
Multifunctional nanoassemblies target bacterial lipopolysaccharides for enhanced antimicrobial DNA delivery / Montis, Costanza; Joseph, Pierre; Magnani, Chiara; Marín-Menéndez, Alejandro; Barbero, Francesco; Ruiz Estrada, Amalia; Nepravishta, Ridvan; Angulo, Jesus; Checcucci, Alice; Mengoni, Alessio; Morris, Christopher J.; Berti, Debora. - In: COLLOIDS AND SURFACES. B, BIOINTERFACES. - ISSN 0927-7765. - ELETTRONICO. - 195:(2020), pp. 111266.1-111266.10. [10.1016/j.colsurfb.2020.111266]

Availability:
This version is available at: https://hdl.handle.net/11585/767442 since: 2020-08-04

Published:

DOI: http://doi.org/10.1016/j.colsurfb.2020.111266

Terms of use:

Some rights reserved. The terms and conditions for the reuse of this version of the manuscript are specified in the publishing policy. For all terms of use and more information see the publisher's website.

This item was downloaded from IRIS Università di Bologna (https://cris.unibo.it/).
When citing, please refer to the published version.

(Article begins on next page)

04 May 2024

This is submitted version of:

Costanza Montis, Pierre Joseph, Chiara Magnani, Alejandro Marín-Menéndez, Francesco Barbero, Amalia Ruiz Estrada, Ridvan Nepravishta, Jesus Angulo, Alice Checcucci, Alessio Mengoni, Christopher J. Morris, Debora Berti

Multifunctional nanoassemblies target bacterial lipopolysaccharides for enhanced antimicrobial DNA delivery

Colloids and Surfaces B: Biointerfaces Volume 195, November 2020, 111266

The final published version is available online at:
https://doi.org/10.1016/j.colsurfb.2020.111266

Multifunctional Nanoassemblies Target Bacterial Lipopolysaccharides for Enhanced Antimicrobial DNA Delivery

Costanza Montis[†], *Pierre Joseph*[‡], *Chiara Magnani*[†], *Alejandro Marín-Menéndez*[§], *Francesco Barbero*[⊥], *Amalia Ruiz Estrada*[¶], *Ridvan Nepravishta*[¶], *Jesus Angulo*[¶], *Alice Checcucci*[∥], *Alessio Mengoni*[∥], *Christopher J. Morris*[¶]*, *Debora Berti*[†]*

[†] Department of Chemistry and CSGI, University of Florence, Florence, Italy. [‡] LAAS-CNRS, Université de Toulouse, CNRS, Toulouse, France. [¶] School of Pharmacy, University of East Anglia, Norwich, UK, [§] Procarta Biosystems Ltd, Norwich Innovation Centre, Norwich, UK, [⊥]Nanovector s.r.l., Turin, Italy, [∥]Department of Biology, University of Florence, Florence, Italy.

Corresponding Authors: *Christopher J. Morris, Christopher.J.Morris@uea.ac.uk; *Debora Berti, debora.berti@unifi.it

Present Addresses: A.M.M. CRCN, MIVEGEC (UM-CNRS 5290-IRD 224) Montpellier, France; F.B. Catalan Institute of Nanoscience and Nanotechnology (ICN2), Barcelona, Spain; C. Magnani LPCM, CIRMAP, University of Mons, Mons, Belgium. A. R. E. School of Pharmacy – Queen's University Belfast, Belfast, UK; R.N. Department of Biochemistry & Molecular Biology, University of Texas Medical Branch, TX, USA; J.A. Departamento de Química Orgánica, Universidad de Sevilla, Sevilla, Spain.

Total number of words: 7063
Total number of tables/figures: 7

HIGHLIGHTS

- Antibacterial 12-bis-THA/TFD hybrid nanoplexes are investigated
- Nanoplexes-bacteria interaction are studied using membrane models and live cells
- 12-bis-THA targets and sequesters LPS, delivering anti-inflammatory activity
- 12-bis-THA-LPS interaction facilitates the entry of antimicrobial TFD in bacteria
- Versatile nanoplexes against Gram -ve bacteria are a promising therapeutic option

ABSTRACT The development of new therapeutic strategies against multidrug resistant Gram-negative bacteria is a major challenge for pharmaceutical research. In this respect, it is increasingly recognized that an efficient treatment for resistant bacterial infections should combine antimicrobial and anti-inflammatory effects. Here, we explore the multifunctional therapeutic potential of nanostructured self-assemblies from a cationic bolaamphiphile, which target bacterial lipopolysaccharides (LPSs) and associates with an anti-bacterial nucleic acid to form nanoplexes with therapeutic efficacy against Gram-negative bacteria. To understand the mechanistic details of these multifunctional antimicrobial-anti-inflammatory properties, we performed a fundamental study, comparing the interaction of these nanostructured therapeutics with synthetic biomimetic bacterial membranes and live bacterial cells. Combining a wide range of experimental techniques (Confocal Microscopy, Fluorescence Correlation Spectroscopy, Microfluidics, NMR, LPS binding assays), we demonstrate that the LPS targeting capacity of the bolaamphiphile self-assemblies, comparable to that exerted by Polymixin B, is a key feature of these nanoplexes and one that permits entry of therapeutic nucleic acids in Gram-negative bacteria. These findings enable a new approach to the design of efficient multifunctional therapeutics with combined antimicrobial and anti-inflammatory effects and have therefore the potential to broadly impact fundamental and applied research on self-assembled nano-sized antibacterials for antibiotic resistant infections.

KEYWORDS Nanomedicine, Antibiotic Resistance, Transcription Factor Decoys, Giant Unilamellar Vesicles, Biomimetic Membranes

INTRODUCTION

The rising resistance of bacteria to antibiotics is recognized as a major healthcare issue that, together with the scarcity of new therapeutic approaches, mandates the development of new antimicrobials acting upon novel bacterial targets[1]. Recently, the World Health Organization (WHO) published a list of antibiotic-resistant "priority pathogens", a catalogue of 12 families of bacteria that pose the greatest threat to human health, for which immediate research effort is required[2]. The list highlights the threat of resistant Gram-negative bacteria including *Acinetobacter*, *Pseudomonas* and various *Enterobacteriaceae* that are resistant to multiple antibiotics including last-resort agents such as carbapenems and third generation cephalosporins.

The inherent antimicrobial resistance of Gram-negative bacteria is related to their unique structure: differently from Gram-positive ones, cell walls of Gram-negative bacteria are characterized by the presence of an asymmetric outer membrane containing >70% w/w of lipopolysaccharides (LPSs), the general structure of which is sketched in Figure 1. LPS consists of an immunogenic lipid portion embedded in the outer leaflet of the lipid bilayer (Lipid A), which is bound to an oligosaccharide moiety (R-core) and to an outer polysaccharide portion protruding from the membrane (O-antigen).[3,4] This thick and highly anionic layer, strongly anchored to the underlying membrane, acts as an efficient xenobiotic permeability barrier[5]. Besides its effects on bacterial resistance, LPS (also called endotoxin), when present in the bloodstream, can trigger uncontrolled inflammatory responses of the host, eventually leading to sepsis and death from septic shock.

A rational approach to the development of effective therapeutics for systemic Gram-negative bacterial infections might include targeting of LPS for the dual purpose of enhancing cellular delivery of antimicrobial agents as well as blocking the immune response in advance of the onset of inflammation and sepsis. It has been recently demonstrated that the coagulation-related peptide, thrombin, binds and sequesters LPS, leading to accelerated aggregation and

phagocytic clearance of *E. coli* bacteria by macrophages *in vitro*.[6] More generally, LPS targeting, binding and removal from the circulation is an innate anti-inflammatory strategy prevalent in species spanning invertebrates to higher mammals. For example, host defense peptides or antimicrobial peptides (AMPs) are an intrinsic component of the innate immune system and are characterized by a broad-spectrum antimicrobial and anti-inflammatory activity.[7] As such, these peptides have received much attention as potential alternatives to traditional antibiotics. [8,9]

In previous studies we presented a nanostructured antimicrobial, made of a cationic bolaamphiphile (12-bis-THA, the structure of which is displayed in Figure 1a) associating with a Transcription Factor Decoy (TFD), an aptamer designed to interfere specifically with the gene transcription mechanisms of the bacteria, to form nanosized complexes (hereafter termed loaded nanoplexes, LNP). Delivery of therapeutic TFDs to pathogenic bacteria is contingent upon co-formulation with the self-assembling 12-bis-THA amphiphile, which binds to and efficiently protects from nuclease degradation the DNA component[10].

LNPs have been shown to be a promising antimicrobial system against both Gram-positive and Gram-negative bacteria[10,11]. Their antibacterial efficacy is attributable to two distinct functions: first, a generic antimicrobial action of the cationic bolaamphiphile, interacting with and weakening cardiolipin-rich bacterial membranes; and secondly, a specific antimicrobial activity of the TFD towards selected genes involved in vital cellular functions of bacteria, such as metabolism and replication.[10] There is also an absence of known transcription factor-mediated resistance pathways, which is a clear advantage over many conventional antibiotic targets. Besides TFD complexation and delivery, the amphiphilic and cationic nature of 12-bis-THA, features shared with AMPs, makes these nanoplexes attractive as a possible LPS targeting species and for anti-inflammatory and antimicrobial purposes in the treatment of Gram-negative bacterial infections.

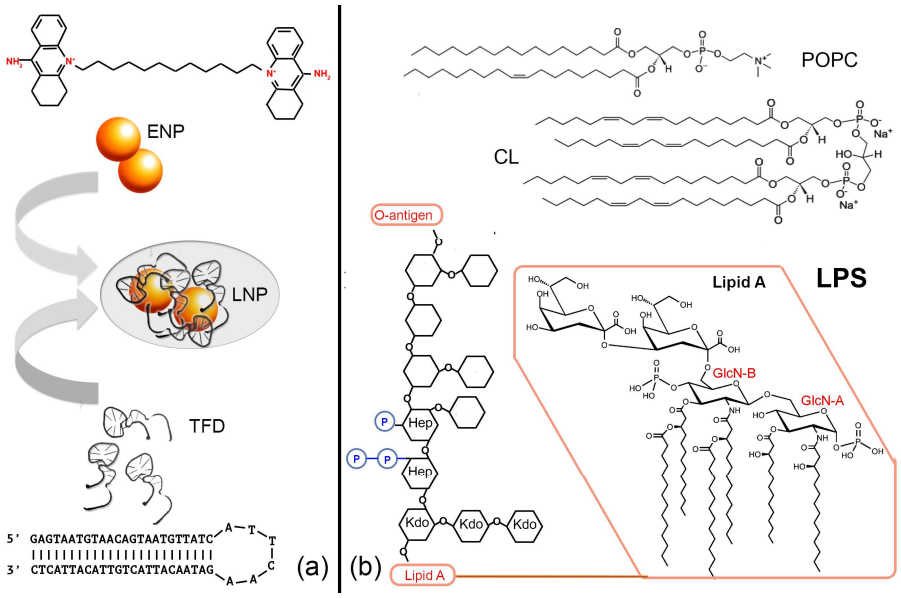

Figure 1. Systems under investigation. (Panel a) Antimicrobial nanoplexes: structure of the 12-bis-THA cationic bolaamphiphile (whose assemblies are named empty nanoplexes, ENP); representative structure of a hairpin Transcription Factor Decoy (TFD); scheme sketching TFD and 12-bis-THA interaction to form loaded nanoplexes (LNPs). (Panel b) Membrane models: structure of the lipids employed in the membrane models: 1-palmitoyl-2-oleoyl-sn-glycero-3-phosphocholine (POPC) and Cardiolipin (CL); general structure of a Lipopolysaccharide (LPS), with the polysaccharide skeleton and the Lipid A moieties highlighted. Hep: Heptulose (ketoheptose); Kdo: 3-deoxy-α-D-mannooctulosonic acid; P: phosphate.

In this report, we perform a fundamental study on the interaction of LNPs with biomimetic and *in vivo* bacterial membranes, in order to explore and understand their potential as multifunctional experimental therapeutics for the treatment of Gram-negative bacterial infections. In this respect, our aim is twofold: first, to specifically investigate 12-bis-THA-TFD nanoplexes as possible antimicrobial and anti-inflammatory systems for Gram-negative bacterial infections; second, to contribute, more generally, to the progress of the fundamental knowledge on the interaction of antimicrobials with Gram-negative bacteria, which will help in the design of more efficient multifunctional therapeutics. To this aim, we study the interaction of LNP with synthetic mimics of Gram-negative bacteria, from two complementary standpoints: (i) bacterial membrane destabilization to achieve an efficient delivery of the

specific antimicrobial TFD into the bacterial cytoplasm (ii) LPS binding and sequestration for anti-inflammatory properties.

An ensemble of experimental techniques, spanning the colloidal length scale down to molecular scale interactions, were combined to demonstrate that LNPs are a versatile system that destabilizes the bacterial outer membrane, promoting cell entry of the antimicrobial TFD, as well as exerting anti-inflammatory action through LPS sequestration. Therefore, LNPs represent multifunctional, tunable, colloidal systems with potential therapeutic efficacy against Gram-negative bacterial pathogens. As such, they have the potential to offer tailored anti-infective treatment in healthcare settings that are increasingly challenged with antibiotic-resistant pathogens.

RESULTS AND DISCUSSION

Interaction of nanoplexes with biomimetic Gram-negative bacterial membranes: Confocal Microscopy and Microfluidics

In order to examine the interaction of LNPs with bacterial cell models, we prepared Giant Unilamellar Vesicles (GUVs) of different and controlled compositions, mimicking either Gram-negative or Gram-positive bacteria and challenged them with LNP. GUVs are primitive mimics not able to fully reproduce the complexity of natural membranes, however, their synthetic nature, allowing a fine control over their composition, geometry and environment, makes them a valuable model to investigate cell-membrane-related phenomena in simplified conditions, both related to eukaryotic[12,13] and to bacterial cells [14,15] ; here we employ GUVs containing the basic components of bacterial membranes, to assess the roles of individual lipid components in the cellular response to the nanoplexes.

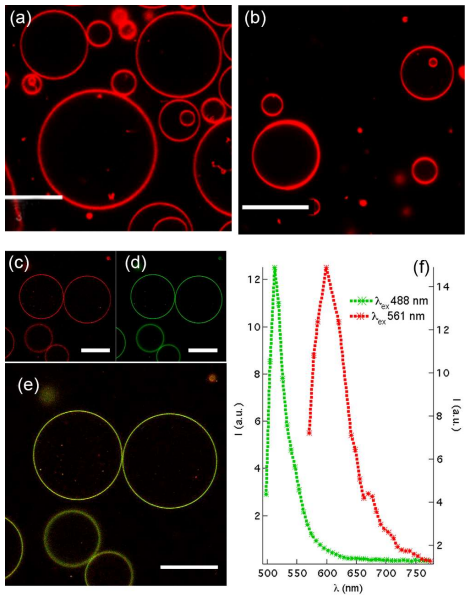

Figure 2. Biomimetic bacterial model membranes. (a-e) Confocal microscopy images of GUVs made of: (a) POPC with 10% w/w CL and (b-e) POPC with 10% w/w CL, plus 17% w/w LPS: (a, b) representative images of GUVs containing the fluorescent tag Liss Rhod PE (red); (c-e) representative images of GUVs of POPC with 10% w/w CL, plus 17% w/w LPS containing the fluorescent lipid tags Bodipy (green) and Alexa-568-conjugated LPS (red) (the separated red (c) and green (d) channels and channel overlays (e) are displayed); (f) spatially resolved emission spectra at λ_{exc} 488 nm (green curve, excitation/emission of Bodipy) and λ_{exc} 561 nm (red curve, excitation/emission of Alexa-568-conjugated LPS) acquired on the same GUV membrane, highlighting the colocalization of the fluorescent tags. Scale bars 30 μm.

As bacterial membrane mimics, we prepared GUVs composed of POPC and cardiolipin (CL), including or excluding 17% w/w LPS from *E. coli*. While CL is a membrane-specific lipid present both in Gram-positive and Gram-negative bacteria, LPS is unique to Gram-negative membranes and is of paramount relevance in determining the inefficacy of many antibacterial treatments. Figure 2 shows some representative Confocal Microscopy (CLSM) images of the Gram-positive POPC-CL model (Figure 2a) and the Gram-negative POPC-CL-LPS model (Figure 2b) GUVs, containing 0.1% mol:mol Liss Rhod PE, a fluorescent lipid, embedded in the lipid bilayer (red). The GUVs' sections are visible as perfectly rounded circles, with Liss Rhod PE staining the lipid membrane shell. While the shape and size of the GUVs is similar in the absence and in the presence of LPS, a significant efficiency decrease of GUV's yield prepared with the usual electroformation procedure was observed in the latter case, probably

due to the higher complexity of the lipid mixture and the increase of negatively charged species to be incorporated in the lipid assembly. In order to check the efficient incorporation of LPS in GUV membranes, we employed a fluorescently labeled LPS. Figure 2c-e display representative CLSM images of GUVs containing both the lipid fluorescent probe Bodipy (green) and Alexa 568-labeled LPS (red) shown both as separate (2c, d) and overlaid (2e) channels. The colocalization of the fluorescence emission of the two probes confirms the successful inclusion of LPS in the GUVs, corroborated by the spatially resolved emission spectra (Figure 2f) acquired on the same GUV lipid membrane regions.

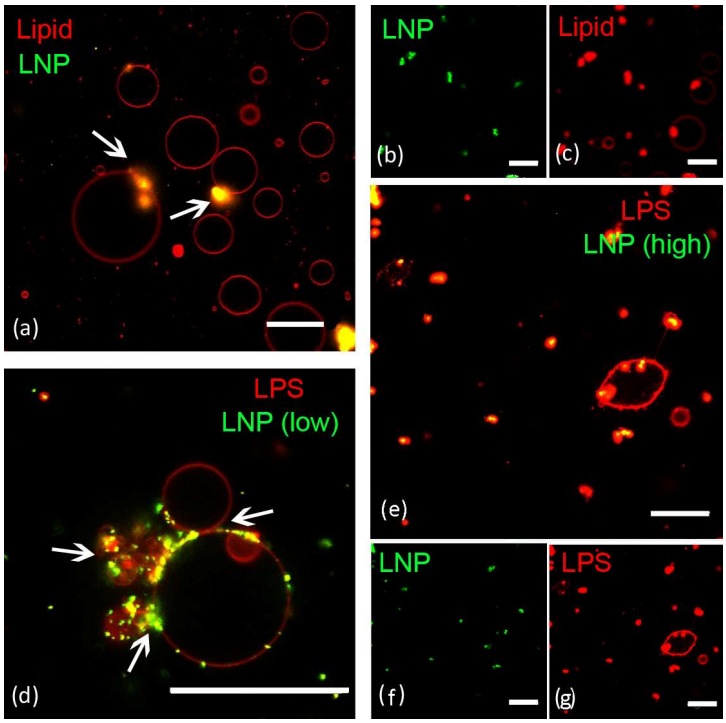

Figure 3. Interaction of LNPs with biomimetic membrane models: CLSM images of GUVs fluorescently labeled with Liss Rhod PE (red) of: (a-c) POPC with 10% w/w CL and (d-g) with the same composition, plus 17% w/w LPS; 120 µL GUVs prepared as described in the experimental section, upon incubation with 20 µL (a-d) and 100 µL (e-g) of LNPs standard solution containing a fluorescent TFD (green); both separate channels and overlayed channels are displayed, with fluorescence colocalization areas seen in yellow. Scale bars 30 µm.

Figure 3 displays some representative CLSM images of 120 µL GUVs (0.03 µg/µL lipid content, with or without LPS,), challenged with 100 µL of an aqueous dispersion of LNPs (0.18

mM 12-bis-THA and 10 μg/μL TFD), containing an AlexaFluor 488-labeled TFD (green). In this medium, LNPs have a size of 200 nm, and a zeta-potential in the order of +30 mV, similar to what previously shown[16]. When GUVs of POPC-CL were used, LNP docked at GUV membranes and fused with them after 2 h incubation (Figure 3a-c); in addition, part of the lipid probe originally staining the GUVs bilayer migrated into the aggregates (white arrows, Figure 3a). This proves a close interaction between the LNPs and the GUVs, also in the absence of lipopolysaccharides in the GUVs, which is expected considering the negative charge of CL (see Figure 1b), and the positive z-potential of the nanoplexes.

However, even low concentrations of LNPs, when added to GUVs containing LPS (Figure 3d), displayed extensive docking and fusion with the GUV membranes. Especially noticeable were extended regions of colocalization of the red lipid label with the green TFD and a clustering of the GUVs with LNPs acting as intervesicular bridges (white arrows, Figure 3d). These interactions were more pronounced with higher concentration of the LNPs (Figure 3 e-g), with many GUVs completely disrupted and the remaining ones extensively deformed and collapsed. To conclude, the presence of the LPS determines much more striking interactions between LNPs and the model lipid membranes. This effect is quite unexpected, considering that LPS act as a protective layer in Gram-negative bacteria, hindering the docking and penetration of exogenous species on bacterial membrane and, ultimately, their entry inside the bacterium.

In order to understand the dynamic aspects of this interaction and better elucidate the GUV membrane disruption, we shifted our focus from static to dynamic experiments, monitoring the LNP-GUV interaction kinetics with confocal microscopy imaging combined with a customized microfluidic configuration, designed to trap and challenge GUVs with a solution[17].

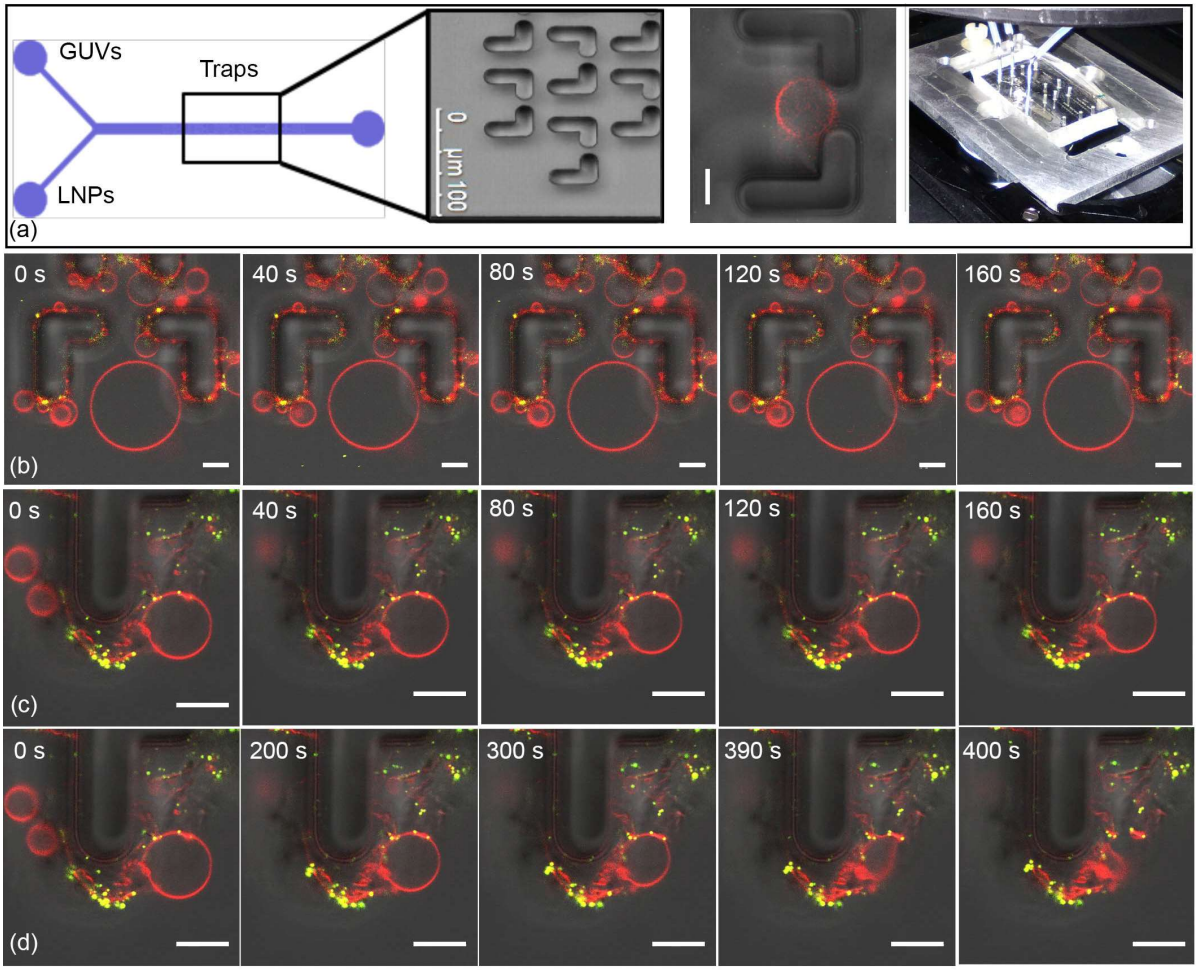

Figure 4. Interaction of LNPs with target membranes: Microfluidics. (a) Experimental set-up for the microfluidics experiment; (b-d) representative CLSM time lapse images of (b) POPC-CL and (c, d) POPC-CL-LPS GUVs labeled as described in the main text in a 160 s (b, c) and 400 s (d) timescale; the overlay of Liss Rhod PE and Alexa 488 fluorescence, with colocalization area highlighted (yellow), and bright field (greyscale) are displayed. Scale bars 10 µm.

Briefly, a PDMS (polydimethylsiloxane) microfluidic chip consisting of two inlets was secured upon a coverglass. Through the first inlet we injected the GUV's dispersion, while the second one was for the subsequent injection of LNP dispersions (Figure 4a). From the first inlet, the injected GUVs flow through a microfluidic channel of 50 µm thickness and 350 µm width containing a series of U-shaped traps at defined channel positions. After GUVs trapping, LNPs stained with an Alexa 488-labeled TFD (green) were injected and the interaction monitored in real time. First, it should be highlighted that an optimal trapping of the GUVs inside the U-shaped obstacles was challenging due to adhesion effects of LNPs on the channel walls and on

GUVs. Nevertheless, striking and unambiguous differences were observed in the absence and in the presence of LPS (compare the time evolution in Figures 4b and c). In the absence of LPS (Figure 4b), the docking of the LNPs at the GUV membrane was clearly visible, although no modifications in the shape of the GUVs were visible over a total LNP exposure time of 160 seconds, which is consistent with the results of static CLSM observations. Conversely, in the presence of LPS (Figure 4c, d), there was a high tendency of the GUVs to interact extensively with LNPs, eventually causing the shrinkage of GUVs (Figure 4c) and, for longer interaction times (Figure 4d), even the implosion of the GUVs, probably due to a lipid extraction effect of the LNPs aggregates (see Supplementary Movies). Interestingly, the shrinkage and implosion of GUVs was observed only when LPS was included in the membrane formulation: this suggests that LNPs bind to LPS and extract it from the membrane. Control experiments confirmed that GUVs prepared with and without LPS were both stable throughout the experimental timescale (data not shown).

These observations indicate that, contrary to current knowledge[18], the presence of LPS favors, rather than inhibits, the interaction of nanoplexes with the target GUVs. This finding is particularly interesting for two reasons: first, the dramatic membrane perturbation and local disruption of GUVs suggests a dramatic increase in membrane permeability, which would favor the delivery of TFD into the GUV lumen and might, therefore, favor the antimicrobial effect of LNPs against Gram-negative bacteria; second, the microfluidic experiment points at a specific binding of 12-bis-THA nanoplexes to the LPS component of the lipid membrane and, possibly, its selective extraction, eventually leading to the complete shrinkage of the GUV. This latter effect suggests that 12-bis-THA-TFD nanoplexes could bind and sequester immunogenic LPS, with anti-inflammatory consequences.

Nanoplexes as antimicrobials against Gram-negative bacteria: LPS-dependent delivery of TFD

The antimicrobial activity of LNPs is dependent upon the delivery of TFD into the bacterial cytoplasm, so that vital cellular processes are repressed by competitive inhibition of transcription factor activity[19]. To monitor this ability, we performed a Fluorescence Correlation Spectroscopy (FCS) investigation on the penetration of a fluorescent TFD both into Gram-positive and Gram-negative biomimetic GUV membranes. Figure 5a shows representative FCS profiles acquired for the Alexa 488-labeled TFD alone (blue filled circles) and after interaction with 12-bis-THA, to form LNPs (red empty circles).

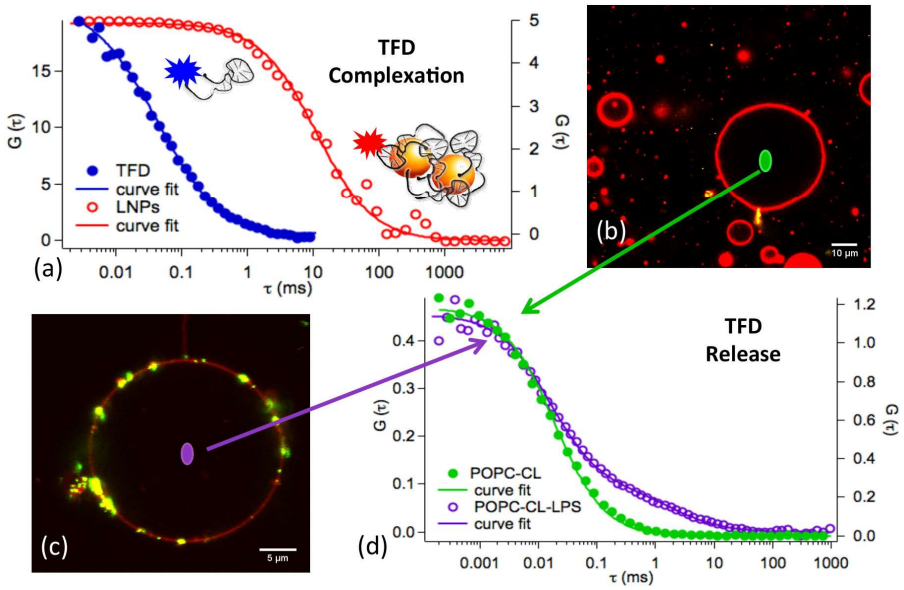

Figure 5. Interaction of LNPs with target membranes: FCS. (a) Representative FCS curves of Alexa 488-labelled TFD (blue filled circles) and of LNPs containing Alexa 488-labelled TFD (red empty circles), curve fitting of the experimental curves (continuous lines); (b, c) representative CLSM images of (b) POPC-CL and (c) GUVs after two hours incubation with LNPs; (d) Representative FCS curves of LNPs containing Alexa 488-labelled TFD measured for POPC-CL GUVs (green filled circles) and for POPC-CL-LPS GUVs (purple empty circles), inside GUVs' lumen (as highlighted with colored spots in (b,c)). The continuous lines display the curve fitting of the experimental curves.

The FCS curve of the TFD could be analyzed with a two-component, three-dimensional normal diffusion model (see SI equation S5)[20–23], where the fast component has a diffusion coefficient D_1 of 370 ± 40 $\mu m^2 s^{-1}$,while the slow component is characterized by D_2 = 60 ± 20 $\mu m^2 s^{-1}$. The slower component is consistent with the diffusion of the dye conjugated to the oligonucleotide, while the fast component is clearly due to a small percentage of the dye not conjugated to the oligonucleotide, possibly through unavoidable nuclease contamination during non-sterile experimental procedures. However, through FCS these two components can be easily, reliably and precisely distinguished. In the presence of the bolaamphiphile, the TFD diffusion is clearly slowed down, due to the 12-bis-THA complexation with DNA and formation of nanoplexes. The diffusion coefficient of the complexed TFD, within the limits of accuracy of this experimental technique for objects of comparable size with respect to the size of the detection volume (see SI equation 3)[21], can be evaluated as: D= 1.9 ± 1 $\mu m^2 s^{-1}$, consistent with nanoplexes of around 200 nm hydrodynamic diameter (SI equation S4).

The LNPs were next incubated with the model Gram-positive cytoplasmic membrane, POPC-CL (Figure 5b) and the model Gram-negative membranes, POPC-CL-LPS (Figure 5c) GUVs. Figure 5b and 5c report some representative CLSM images, consistent with the previously discussed phenomena (see Figure 3-4). In brief, LNPs interact closely with the lipid membrane of GUVs, docking and eventually fusing into it. However, no TFD accumulation is observed inside the GUVs' lumen, and the LNPs' aggregates remain largely confined on the surface of the lipid membrane. FCS measurements were performed inside POPC-CL and POPC-CL-LPS GUVs in order to verify if TFD, in complexed or free form, is released inside the GUVs'. Figure 5d shows the FCS curves acquired inside POPC-CL GUVs' (green filled markers) and inside POPC-CL-LPS GUVs' (purple empty markers), respectively. For POPC-CL GUVs the measured FCS profile can be interpreted according to a 1-component 3D fitting model, due to the sole presence of the free dye (D = 370 $\mu m^2 s^{-1}$). For POPC-CL-LPS GUVs a second longer

decay is present. Using a two-component model, in which the fast-diffusing component is fixed at D = 370 $\mu m^2 s^{-1}$, an estimate of the LNP intra-luminal diffusion coefficient was determined as D = 2.9 ± 0.6 $\mu m^2 s^{-1}$. These observations indicate that the presence of the LPS on the lipid membrane not only promotes the interaction of the LNPs with the GUVs' membrane, but also permits internalization of the nanoplexes smaller than the original ones (average hydrodynamic diameter 150 nm), suggesting a partial decomplexation when the LPS-containing membrane is crossed.

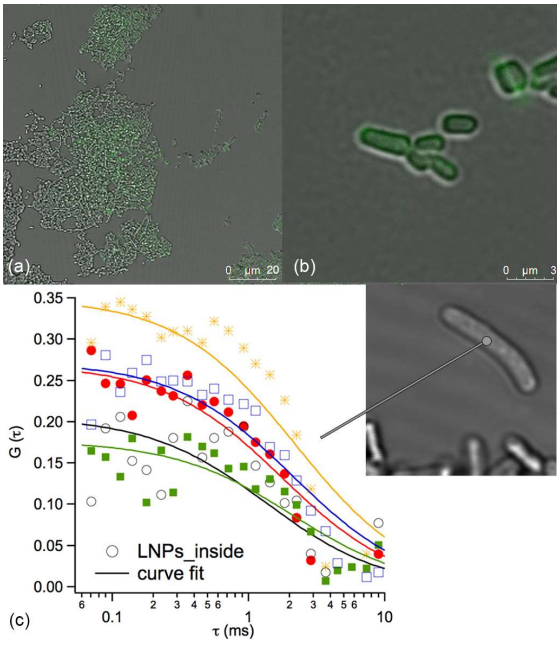

Figure 6. Interaction of LNPs with live bacteria: FCS. (a, b) Representative CLSM images of *E. coli* bacteria upon incubation with LNPs containing Alexa 488-labelled TFD, Alexa 488 fluorescence (green) and bright field (greyscale) overlay; (c) five representative FCS curves of LNPs containing Alexa 488-labelled TFD measured inside *E. coli* cytoplasm (empty and filled markers), curve fit of the experimental data (continuous lines). The inset of (c) shows a representative brightfield CLSM image of *E. coli* cytoplasm where FCS has been measured.

In order to corroborate the data gathered on bacterial membrane mimics, we performed FCS on a live model Gram-negative bacterium, *E. coli*, to monitor the penetration of the fluorescently-labeled TFD into the bacterial cytoplasm. Clearly, FCS measurements on bacteria are particularly challenging due to the detection volume, which, in the z direction, is

slightly larger than the bacterium size. This latter limitation does not allow a precise estimate of the diffusion coefficient inside the detection volume. *E. coli* bacteria were challenged with LNPs containing Alexa 488-labeled TFD. After 1h 30' incubation at r.t. the bacteria were extensively washed in order to exclude surface-bound LNPs from the analysis. Figures 6a, b show the CLSM images of *E. coli* after incubation with LNPs: the green fluorescence of the Alexa 488-labeled TFD inside the bacterial cytoplasm suggests the successful uptake of TFD. Figure 6c displays five representative FCS curves acquired inside the bacterial cytoplasm of different *E. coli* cells. The clearly visible correlation decay is due to the diffusion of the TFD inside the bacterial cytoplasm. However, the FCS profiles were generally noisy, due to the complex and heterogeneous intracellular environment, united with a low fluorophore concentration. From these data, the reliable determination of a diffusion coefficient (and possibly a hydrodynamic size) is not possible. However, by fitting the experimental curves as due to a single component 3D diffusion, a diffusion coefficient of about 5 ± 2 $\mu m^2 s^{-1}$ was inferred. This value is one order of magnitude higher than the diffusion coefficient of a lipidated Bodipy probe (molecular mass ~ 500 Da) sequestered in the cytoplasmic membrane of *E. coli* [24] and determined through FRAP (D= 0.6 ± 0.2 $\mu m^2 s^{-1}$). This supports the claim that the fluorescent species diffuses in the cytoplasm, rather than the cell membrane, which has a considerably higher effective viscosity. In addition, if we compare this result with the diffusion coefficient obtained inside the LPS-containing GUVs (D = 2.9 ± 0.6 μm^2s-1) and take into account that the bacterial cytoplasm is characterized by a higher viscosity with respect to water[24–26], we can conclude that inside the bacteria the TFD is, at least partially, decomplexed.

Overall, these experiments prove the significant role of LPS in promoting membrane permeabilization and subsequent TFD delivery inside cells' cytoplasm, upon interaction with LNPs.

Nanoplexes as anti-inflammatory agents: LPS binding and sequestration.

The observations highlighted above prompted us to investigate the mechanism of LPS sequestration by 12-bis-THA and its biological consequences. Using saturation transfer difference (STD) NMR spectroscopy[27] we sought to examine, at the molecular level, the extent and specificity of 12-bis-THA binding to liposomes of DOPC (1,2-dioleoyl-sn-glycero-3-phosphocholine) in the absence and in the presence of LPS, taken as model membranes. STD NMR is appropriate for studying small-molecule binders of weak-medium affinity to large target molecules[28]. Through saturation of the target "receptor" molecule (which in this study is LPS bound to a liposome surface) and by studying the transfer to a bound ligand (here represented by 12-bis-THA), a map of ligand-receptor binding sites can be constructed. No STD signals were observed for samples containing 12-bis-THA and pure DOPC liposomes (Figure 7a, blue spectrum) indicating the absence of interaction in this system. In sharp contrast, many STD peaks were observed with DOPC liposomes containing LPS (Figure 7a, red spectrum), indicating extensive interaction between LPS-decorated liposomes and 12-bis-THA (reference spectrum for which is shown in green, Figure 7a). The STD NMR technique affords an exquisite insight into the ligand domains that bind to a target macromolecule through the comparison of the extents of STD for different resonances after irradiation at different "receptor" frequencies[29]. For example, irradiation of LPS at different frequencies such as -4 ppm for the lipophilic core, or 4.9 ppm and 5.2 ppm for the glucosamine rings GlcN-B and GlcN-A of LPS (Figure 1b), permits the construction of an epitope binding map, detailing the proximity of 12-bis-THA protons to the LPS binding site (Figure 7b). Careful analysis identified the orientation of the protons labeled here as C, E, I, F and K toward GlcN-A and GlcN-B (highlighted in Fig 1b). This region presents a positive charge located on the Nitrogen atom, which presumably makes contact with the negative charge located on the GlcN-A

orienting the head protons H, G, A, B, D away from this contact point (details of the binding orientation are in the Supplementary Information). It is also interesting to note that the protons labeled as M and N located in the center of the symmetrical linker, are oriented toward the aliphatic chains of DOPC/LPS liposome (Figure 7b). Following these arguments, one may conclude that the binding region of the 12-bis-THA on the LPS is centered on the GlcN-A negative charge, establishing close proximity with the positively charged Nitrogen atom at the polar head of 12-bis-THA, while the central protons of the lipophilic linker interact closely with the aliphatic region of the DOPC/LPS liposome. These data indicate that the interaction between 12-bis-THA and LPS is specific and not solely attributable to charge compensation.

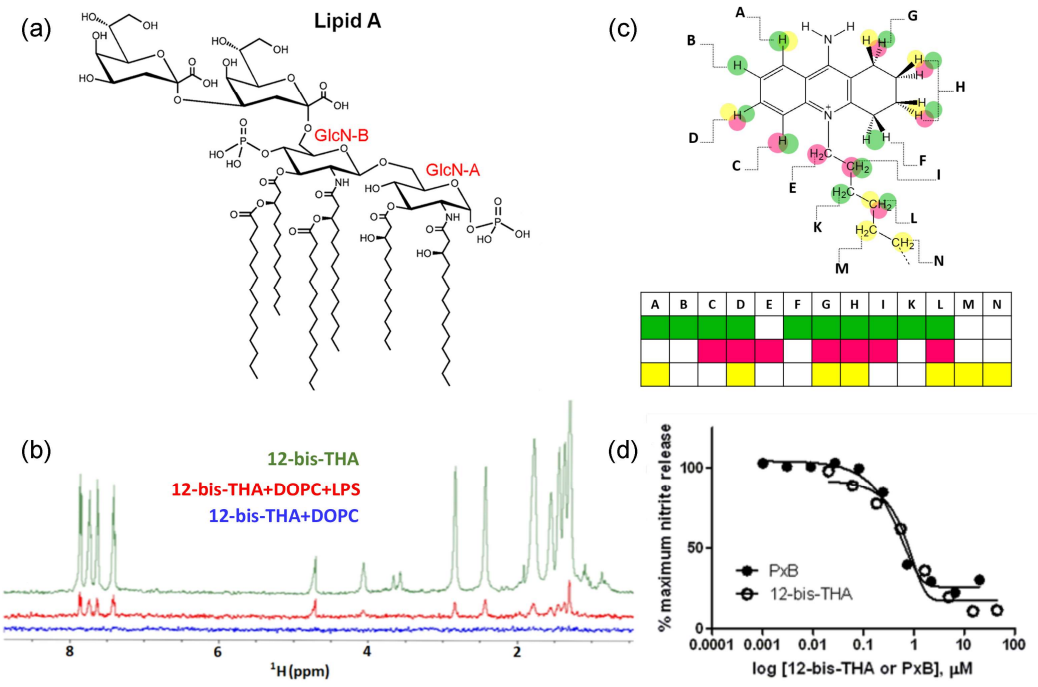

Figure 7: Binding of 12-bis-THA to LPS and its biological effects. (a) Structural formula of Lipid A (b) STD-NMR spectra of 12-bis-THA (400 µM) alone (green), in the presence of DOPC liposomes (blue) or DOPC:LPS liposomes (red). (c) Structural formula of one half of the symmetrical 12-bis-THA molecule overlaid with colored circles indicating proton orientation in LPS-containing model membranes. Green are protons oriented toward GlcN-A; magenta are protons oriented toward GlcN-B; yellow are protons oriented toward the aliphatic chains of DOPC/LPS liposome. (d) Dose-dependent effects of 12-bis-THA (empty circles) and PxB (filled circles) on nitric oxide release by RAW 264.7 macrophages, determined by Griess assay of media nitrite levels. Data are mean of 3 independent experiments. Error bars are omitted for clarity.

Functional neutralization of LPS by 12-bis-THA was confirmed by *in vitro* studies with mouse RAW 264.7 macrophage cells. We challenged macrophages with *E. coli* LPS in the presence or absence of escalating concentrations of 12-bis-THA or polymyxin B (PxB), which was deployed as a gold standard LPS binder[30] used in the clinic as both an antibiotic[31] and endotoxin removal tool[32]. LPS-only controls consistently increased the nitrite concentration of the culture medium to > 10 μM. The co-application of 12-bis-THA with LPS caused a concentration-dependent decrease in nitrite concentration, indicating reduced nitric oxide by macrophage cells i.e. an anti-inflammatory effect mediated through LPS sequestration. Strikingly, 12-bis-THA assemblies and PxB were of comparable potency at inhibiting nitric oxide release from macrophages in response to LPS (Figure 7c) with IC_{50} values of 5.1 and 0.5 μM, respectively. The viability of macrophage cells was not compromised across the 10 nM - 100 μM concentration range tested, as judged by MTT assay (Supplementary Figures). These results indicate that the extracellular binding of LPS by 12-bis-THA is sufficient to prevent the acute pro-inflammatory response mediated through the cell surface toll-like receptor 4 receptor complex and the downstream inducible nitric oxide synthase (iNOS). Confiscation of blood-circulating LPS in septic patients is a key research priority in light of the increasing number of Gram negative bacterial sepsis deaths worldwide[33]. The neutralization of LPS is a highly desirable characteristic that has been pursued by a number of groups who have employed a range of different scaffolds spanning the small and macromolecular size ranges [34–38].

CONCLUSIONS

In this study we investigated the interaction of the nanostructured, antimicrobial 12-bis-THA-TFD nanoplexes (LNPs) with Gram-positive and Gram-negative bacterial biomimetic membranes. We found that the interaction between the LNPs and Gram-negative bacteria critically involves LPS binding to 12-bis-THA nanoplexes which favors the docking of LNPs

to the bacterial membrane. These LNP-LPS interactions lead to two phenomena, both of paramount importance to future application of LNPs as efficient and multifunctional therapeutics for Gram-negative infections: (i) they induce membrane destabilization and increase membrane permeability, allowing the efficient delivery of antimicrobial TFDs into the bacterial cytoplasm; (ii) they afford LPS binding and sequestration, with its associated anti-inflammatory effects, comparable with the golden standard PxB. These results demonstrate that the combination of 12-bis-THA and the TFD into nanoplexes represents a promising strategy to tackle Gram-negative bacterial infections, with a synergistic, multifunctional approach. In addition, the mechanistic insights on the interaction between nanoplexes and Gram-negative bacterial membrane models can be exploited to predict the antimicrobial-anti-inflammatory behavior of different formulations based on cationic amphiphiles and nucleic acids and, therefore, will provide useful basic information for the design of novel effective therapeutics against antimicrobial resistant Gram-negative bacterial infections. Key mutations in LPS biosynthesis, such as sugar phosphorylation, lipid A modification or O-antigen deletions have been identified in Gram negative bacteria such as Pseudomonas aeruginosa isolated from chronically infected cystic fibrosis patients[39]. Binding between 12-bis-THA and mutant LPS from antimicrobial resistant Gram-negative bacteria as well as antibacterial activity is the subject of ongoing research and will be reported elsewhere. The concomitant anti-inflammatory activity of LNPs contributes a second, highly attractive attribute to this new drug delivery platform, making it an important tool in the fight against antibiotic-resistant pathogens.

EXPERIMENTAL SECTION

Materials

POPC (1-palmitoyl-2-oleoyl-sn-glycero-3-phospho- choline), DOPC (1,2-dioleoyl-sn-glycero-3-phosphocholine), Cardiolipin (sodium salt from bovine heart) and Lipopolysaccharide from Escherichia coli were acquired from Sigma Aldrich (St. Louis MO). 12-bis-THA (1,10-(dodecane-1,12-diyl)-bis-(9-amino-1,2,3,4-tetrahydroacridinium) chloride, MW = 635.6 g/mol) was synthesized by Shanghai Chempartners co. (Denmark) with >98% purity. The TFD and its Alexa-488-labelled version were kindly provided to us by Procarta Biosystems Ltd. (Norwich, UK). Both non-labelled and Alexa 488-labelled oligonucleotide were specifically design to finally obtain a hairpin secondary structure according to the oligo analyser tool (version 3.1) from IDT-DNA free software and confirmed with the DINAMelt Web Server (University at Albany, USA). The lyophilized powder was first suspended in filter sterilised Milli-Q water to a concentration of 1 mg/ml. Once in dilution, the samples were incubated 5 minutes at 95°C and then let to cool down at room temperature to allow the complementary sequences to anneal. Then, there were kept at -20°C until used.

12-bis-THA-TFD nanoplexes (LNP) preparation

The dispersion of 12-bis-THA with chloride counter ion (0.18 mM) in aqueous solution was obtained by first dissolving the compound in milliQ-water. The homogenous dispersion in water was then obtained by vigorous stirring with vortex, leading to the formation of empty nanoplexes (ENPs). Similarly, loaded nanoplexes (LNPs) were obtained by adding the bolaamphiphile dispersion (0.18 mM) to a solution containing the TFD in milliQ-water (10 μg/mL) and stirring the mixture with vortex for 30 seconds. When required, Alexa Fluor 488-labelled TFD was used.

Membrane models preparation

Giant Unilamellar Vesicles were prepared through electroformation, as described elsewhere[40]. Lipid composition was 90% w/w POPC and 10% w/w Cardiolipin (plus 17%

w/w LPS for LPS containing GUVs) and 0.1% (for confocal microscopy imaging) or 0.01% (for Fluorescence Correlation Spectroscopy experiments) with respect to the total lipid amount of the fluorescent dyes (β-Bodipy or Liss Rhod PE) was added. The dispersions of GUVs in 50 mM Sucrose were employed within 24 hours after preparation for CLSM and FCS experiments. Further details are in the SI.

For NMR experiments, 20 mg/mL dispersions of DOPC and DOPC:LPS (50% w/w) liposomes in D_2O, were prepared according to a standard protocol of dry lipid film hydration, freeze-thaw and sonication[41], which is described in details in the SI.

Confocal Laser Scanning Microscopy

CLSM experiments were carried out with a laser scanning confocal microscope Leica TCS SP8 (Leica Microsystems GmbH, Wetzlar, Germany) equipped with a 63x water immersion objective.[42] The 488 nm laser line was employed to detect β-Bodipy fluorescence and Alexa 488-labeled TFD (λ excitation 488 nm, λ emission 498 nm - 530 nm); the 561 nm laser line was employed to detect Liss Rhod PE dye inside the GUVs' membrane or Alexa 568-labeled LPS (λexcitation 561 nm, λ emission 571 nm - 650 nm). Samples containing LNPs and GUVs were incubated for one hour before the acquisition of the images. Further details are in the SI.

Microfluidics experiments

Polydimethylsiloxane (PDMS) - glass microfluidic chips were fabrication is reported in the SI. 50 μL of the solution obtained by electroformation was diluted to 1 mL with a 15 mM aqueous sucrose solution, filtered at 0.2 μm. The obtained solution was injected in one inlet of a Y-shaped microfluidic channel (Figure 4), while a diluted (1:10) LNPs standard solution with Alexa-488-labelled TFD was injected in the other inlet. The flow rates of the injected GUVs and LNPs, ranging from 0.1 to 1 μL/min, were controlled thanks to two syringes connected to

a syringe pump (Nemesys, Cetoni GmbH) by standard tubing (1/16'' OD, 0.81mm ID). In a microfluidic experiment first GUVs were injected at 1 µL/min and LNPs at 0.1 µL/min, to achieve efficient GUVs trapping without significant exposure to LNPs, then the flow rate was reversed to 0.1 µL/min for GUVs and 1 µL/min for LNPs to expose GUVs to LNPs. Chips were put under vacuum for at least 20 min before the experiments to reduce bubble trapping during channel filling. Characterization was achieved by imaging, by Confocal Laser Scanning Microscopy CLSM (Leica TCS SP8).

Fluorescence Correlation Spectroscopy

FCS measurements were carried out using a Leica TCS SP8 confocal microscope (Leica Microsystems GmbH, Wetzlar, Germany) equipped with a PicoQuant FCS modulus (PicoQuant, Berlin, Germany). Measurements were performed using a 63x water immersion objective. The fluorescently-labeled TFD and Rhodamine 110 for calibration of the confocal volume were excited using the 488 nm-laser line of an Ar laser and the fluorescence emission was acquired using a Hybrid SMD detector in the 498–530 nm range.

For experiments on TFD release inside GUVs 120 µL GUVs dispersion in Sucrose was put in measurement wells (Lab-Tek Chambered 1.0 Borosilicate Coverglass System, Nalge Nunc International, Rochester, NY USA) and diluted with 80 µL Glucose 50 mM. 100 µL (for POPC-CL GUVs) or 20 µL (for POPC-CL-LPS GUVs) of LNPs standard solution prepared as previously described, with Alexa-labelled TFD, were added to the dispersion. Samples containing LNPs and GUVs were incubated for one hour before the acquisition of FCS curves inside GUVs lumen.

For FCS experiments on *E. coli* a bacterial dispersion in H_2O was incubated with the same volume of LNPs (prepared with Alexa 488-labeled TFD). To visualize the bacteria in confocal microscopy and to carry out FCS experiments, the bacteria were layered on the bottom of appropriate wells, which were pre-treated with polylysine, to favor bacterial adhesion on the

coverglass. The dispersion of bacteria or bacteria and LNPs was allowed to interact with the polylysine layer for 1h at r.t. in a humidity-controlled chamber, then the supernatant was removed and the bacterial layer inside the wells was extensively washed with H_2O and then diluted with 300 µL H_2O. FCS experiments in bacteria were carried out by focusing with CLSM the confocal volume in the center of cells' cytoplasm and then acquiring FCS curves. All details on FCS data analysis are reported in the SI.

Saturation Transfer Difference NMR spectroscopy

^{1}H NMR Saturation transfer difference experiments were acquired on a Bruker AVANCE 500 MHz at 298K. To a solution of 12-bis-THA 400 µM in D_2O was added a suspension of LPS/DOPC liposomes or only DOPC liposomes in D_2O at the final concentration of 2 µM of LPS considering a MW of 10 kDa for the LPS. Shortly after that, the sample was transferred in 5 mm NMR tubes for spectra acquisition. The saturation transfer difference (STD) experiment was acquired using the Bruker library pulse *stddiffesgp* with a SW of 16 ppm a TD of 32K a relaxation delay (D1) of 6 seconds and a variable time for the train of the selective saturating 90° Gaussian pulse, from 0.5 to 6 s. The spectra were acquired with 32 or 64 scans. The saturation pulse (ON) was positioned in three different regions of the spectra, at -4.0 ppm, 4.9 ppm and 5.2 ppm. These resonances were chosen as representative of the lipophilic core of the LPS/DOPC liposome, GlcN-B and GlcN-A of LPS respectively. The OFF pulse was always positioned at 40 ppm and the spectra obtained were used as a reference. With the aim to obtain insight of the binding orientation of the 12-bis-THA to the LPS the epitope mapping protocol was used. The saturation received from the proton of the ligand is calculated considering the STD build-up curve in a time course experiment using a variable time for the saturation pulse from 0.5 to 6 seconds. The data were fitted to the equation STD=STDmax * (1-exp(-K*t) from where the STD_0 was calculated as STDmax*K = STD_0.[43]

Inhibition of nitric oxide production by macrophage cells

The murine macrophage RAW 264.7 cell line (American Type Culture Collection, USA) was maintained at 37 °C in DMEM supplemented with 10% heat inactivated fetal bovine serum, in a 5% CO_2 incubator. Cells were seeded onto 96 well plates (10^5 per well) and grown overnight. Culture medium was removed and replaced with 0.1 mL fresh medium supplemented with 500 ng *E. coli* LPS alone or LPS combined with escalating concentrations of 12-bis-THA or PxB. After 24 h, media was removed, centrifuged briefly (200 x g, 5 min) to remove any cellular material and then subjected to a Griess Assay[44] to determine media nitrite concentration as an indicator of nitric oxide production by iNOS.

SUPPORTING INFORMATION

Supplementary Materials and Methods (PDF), Microfluidic movie of POPC-CL and POPC-CL-LPS GUVs interacting with LNPs (.avi)

ACKNOWLEDGMENT

The authors thank Prof Michael McArthur (UEA) for providing the LNP components and critically reading the manuscript. This work was partly supported by LAAS-CNRS micro and nanotechnologies platform member of the French RENATECH network. C.M. and P.J. gratefully acknowledge " PICS CNRS Microfluidics for Soft Matter " for funding. This work was funded under the 7-People Framework—Marie Curie Industry and Academia Partnerships & Pathways scheme (grant agreement nr. 612338).

REFERENCES

[1] A.H. Holmes, L.S.P. Moore, A. Sundsfjord, M. Steinbakk, S. Regmi, A. Karkey, P.J. Guerin, L.J.V. Piddock, Understanding the mechanisms and drivers of antimicrobial resistance, Lancet. (2016). https://doi.org/10.1016/S0140-6736(15)00473-0.

[2] World Health Organization website, 5 February 2018, Antibiotic Resistance, (https://www.who.int/en/news-room/fact-sheets/detail/antibiotic-resistance), (n.d.).

[3] A. Schmidtchen, M. Malmsten, Peptide interactions with bacterial lipopolysaccharides, Curr. Opin. Colloid Interface Sci. 18 (2013) 381–392. https://doi.org/10.1016/j.cocis.2013.06.003.

[4] L.A. Clifton, S.A. Holt, A. V. Hughes, E.L. Daulton, W. Arunmanee, F. Heinrich, S. Khalid, D. Jefferies, T.R. Charlton, J.R.P. Webster, C.J. Kinane, J.H. Lakey, An Accurate in Vitro Model of the E. coli Envelope, Angew. Chemie - Int. Ed. (2015). https://doi.org/10.1002/anie.201504287.

[5] A.H. Delcour, Outer membrane permeability and antibiotic resistance, Biochim. Biophys. Acta - Proteins Proteomics. (2009). https://doi.org/10.1016/j.bbapap.2008.11.005.

[6] J. Petrlova, F.C. Hansen, M.J.A. van der Plas, R.G. Huber, M. Mörgelin, M. Malmsten, P.J. Bond, A. Schmidtchen, Aggregation of thrombin-derived C-terminal fragments as a previously undisclosed host defense mechanism, Proc. Natl. Acad. Sci. 114 (2017) E4213–E4222. https://doi.org/10.1073/pnas.1619609114.

[7] R.E.W. Hancock, E.F. Haney, E.E. Gill, The immunology of host defence peptides: Beyond antimicrobial activity, Nat. Rev. Immunol. (2016). https://doi.org/10.1038/nri.2016.29.

[8] A. Schmidtchen, M. Malmsten, (Lipo)polysaccharide interactions of antimicrobial peptides, J. Colloid Interface Sci. 449 (2015) 136–142. https://doi.org/10.1016/j.jcis.2014.11.024.

[9] S. Singh, P. Papareddy, M. Kalle, A. Schmidtchen, M. Malmsten, Importance of lipopolysaccharide aggregate disruption for the anti-endotoxic effects of heparin cofactor II peptides, Biochim. Biophys. Acta - Biomembr. 1828 (2013) 2709–2719. https://doi.org/10.1016/j.bbamem.2013.06.015.

[10] A. Marín-Menéndez, C. Montis, T. Díaz-Calvo, D. Carta, K. Hatzixanthis, C.J. Morris, M. McArthur, D. Berti, Antimicrobial Nanoplexes meet Model Bacterial Membranes: the key role of Cardiolipin, Sci. Rep. 7 (2017) 41242. https://doi.org/10.1038/srep41242.

[11] M. Mamusa, L. Sitia, F. Barbero, A. Ruyra, T.D. Calvo, C. Montis, A. Gonzalez-Paredes, G.N. Wheeler, C.J. Morris, M. McArthur, D. Berti, Cationic liposomal vectors incorporating a bolaamphiphile for oligonucleotide antimicrobials, Biochim. Biophys. Acta - Biomembr. 1859 (2017). https://doi.org/10.1016/j.bbamem.2017.06.006.

[12] R. Dimova, Giant Vesicles and Their Use in Assays for Assessing Membrane Phase State, Curvature, Mechanics, and Electrical Properties, Annu. Rev. Biophys. (2019). https://doi.org/10.1146/annurev-biophys-052118-115342.

[13] M. Laurencin, T. Georgelin, B. Malezieux, J.M. Siaugue, C. Ménager, Interactions between giant unilamellar vesicles and charged core-shell magnetic nanoparticles, Langmuir. (2010). https://doi.org/10.1021/la1023746.

[14] K. Al Nahas, J. Cama, M. Schaich, K. Hammond, S. Deshpande, C. Dekker, M.G. Ryadnov, U.F. Keyser, A microfluidic platform for the characterisation of membrane active antimicrobials, Lab Chip. (2019). https://doi.org/10.1039/c8lc00932e.

[15] T. Anunthawan, C. De La Fuente-Núñez, R.E.W. Hancock, S. Klaynongsruang, Cationic amphipathic peptides KT2 and RT2 are taken up into bacterial cells and kill planktonic and biofilm bacteria, Biochim. Biophys. Acta - Biomembr. (2015). https://doi.org/10.1016/j.bbamem.2015.02.021.

[16] M. Mamusa, C. Resta, F. Barbero, D. Carta, D. Codoni, K. Hatzixanthis, M. McArthur, D. Berti, Interaction between a cationic bolaamphiphile and DNA: The route towards nanovectors for oligonucleotide antimicrobials, Colloids Surfaces B Biointerfaces. 143 (2016) 139–147. https://doi.org/10.1016/j.colsurfb.2016.03.031.

[17] C. Magnani, C. Montis, G. Mangiapia, A.-F. Mingotaud, C. Mingotaud, C. Roux, P. Joseph, D. Berti, B. Lonetti, Hybrid vesicles from lipids and block copolymers: Phase behavior from the micro- to the nano-scale, Colloids Surfaces B Biointerfaces. (2018). https://doi.org/10.1016/j.colsurfb.2018.01.042.

[18] H. Nikaido, Molecular Basis of Bacterial Outer Membrane Permeability Revisited, Microbiol. Mol. Biol. Rev. (2003). https://doi.org/10.1128/MMBR.67.4.593-656.2003.

[19] M. McArthur, M.J. Bibb, Manipulating and understanding antibiotic production in Streptomyces coelicolor A3(2) with decoy oligonucleotides, Proc. Natl. Acad. Sci.

(2008). https://doi.org/10.1073/pnas.0710724105.

[20] J. Ries, P. Schwille, Fluorescence correlation spectroscopy, Bioessays. 34 (2012) 361–368. https://doi.org/DOI 10.1002/bies.201100111.

[21] K. Koynov, H.-J. Butt, Fluorescence correlation spectroscopy in colloid and interface science, Curr. Opin. Colloid Interface Sci. 17 (2012) 377–387. https://doi.org/10.1016/j.cocis.2012.09.003.

[22] D. Schaeffel, R.H. Staff, H.J. Butt, K. Landfester, D. Crespy, K. Koynov, Fluorescence correlation spectroscopy directly monitors coalescence during nanoparticle preparation, Nano Lett. (2012). https://doi.org/10.1021/nl303581q.

[23] C. Montis, A. Zendrini, F. Valle, S. Busatto, L. Paolini, A. Radeghieri, A. Salvatore, D. Berti, P. Bergese, Size distribution of extracellular vesicles by optical correlation techniques, Colloids Surfaces B Biointerfaces. 158 (2017). https://doi.org/10.1016/j.colsurfb.2017.06.047.

[24] A. Nenninger, G. Mastroianni, A. Robson, T. Lenn, Q. Xue, M.C. Leake, C.W. Mullineaux, Independent mobility of proteins and lipids in the plasma membrane of Escherichia coli, Mol. Microbiol. (2014). https://doi.org/10.1111/mmi.12619.

[25] M. Kumar, M.S. Mommer, V. Sourjik, Mobility of cytoplasmic, membrane, and DNA-binding proteins in Escherichia coli, Biophys. J. 98 (2010) 552–559. https://doi.org/10.1016/j.bpj.2009.11.002.

[26] J.T. Mika, G. Van Den Bogaart, L. Veenhoff, V. Krasnikov, B. Poolman, Molecular sieving properties of the cytoplasm of Escherichia coli and consequences of osmotic stress, Mol. Microbiol. 77 (2010) 200–207. https://doi.org/10.1111/j.1365-2958.2010.07201.x.

[27] M. Mayer, B. Meyer, Characterization of ligand binding by saturation transfer difference NMR spectroscopy, Angew. Chemie - Int. Ed. (1999). https://doi.org/10.1002/(SICI)1521-3773(19990614)38:12<1784::AID-ANIE1784>3.0.CO;2-Q.

[28] M. Mayer, B. Meyer, Group epitope mapping by saturation transfer difference NMR to

identify segments of a ligand in direct contact with a protein receptor, J. Am. Chem. Soc. (2001). https://doi.org/10.1021/ja0100120.

[29] S. Monaco, L.E. Tailford, N. Juge, J. Angulo, Differential Epitope Mapping by STD NMR Spectroscopy To Reveal the Nature of Protein–Ligand Contacts, Angew. Chemie - Int. Ed. (2017). https://doi.org/10.1002/anie.201707682.

[30] N. Paracini, L.A. Clifton, M.W.A. Skoda, J.H. Lakey, Liquid crystalline bacterial outer membranes are critical for antibiotic susceptibility, Proc. Natl. Acad. Sci. (2018). https://doi.org/10.1073/pnas.1803975115.

[31] M.E. Falgas, S.K. Kasiakou, L.D. Saravolatz, Colistin: The Revival of Polymyxins for the Management of Multidrug-Resistant Gram-Negative Bacterial Infections, Clin. Infect. Dis. (2005). https://doi.org/10.1097/01.inf.0000174577.97635.7b.

[32] D.N. Cruz, M.A. Perazella, R. Bellomo, M. de Cal, N. Polanco, V. Corradi, P. Lentini, F. Nalesso, T. Ueno, V.M. Ranieri, C. Ronco, Effectiveness of polymyxin B-immobilized fiber column in sepsis: A systematic review, Crit. Care. (2007). https://doi.org/10.1186/cc5780.

[33] I. Chopra, C. Schofield, M. Everett, A. O'Neill, K. Miller, M. Wilcox, J.M. Frère, M. Dawson, L. Czaplewski, U. Urleb, P. Courvalin, Treatment of health-care-associated infections caused by Gram-negative bacteria: a consensus statement, Lancet Infect. Dis. (2008). https://doi.org/10.1016/S1473-3099(08)70018-5.

[34] X. Chen, R.P.M. Dings, I. Nesmelova, S. Debbert, J.R. Haseman, J. Maxwell, T.R. Hoye, K.H. Mayo, Topomimetics of amphipathic β-sheet and helix-forming bactericidal peptides neutralize lipopolysaccharide endotoxins, J. Med. Chem. (2006). https://doi.org/10.1021/jm0610447.

[35] S.A. David, Towards a rational development of anti-endotoxin agents: Novel approaches to sequestration of bacterial endotoxins with small molecules, J. Mol. Recognit. (2001). https://doi.org/10.1002/jmr.549.

[36] S.E. Sestito, F.A. Facchini, I. Morbioli, J.M. Billod, S. Martin-Santamaria, A. Casnati, F. Sansone, F. Peri, Amphiphilic Guanidinocalixarenes Inhibit Lipopolysaccharide (LPS)-and Lectin-Stimulated Toll-like Receptor 4 (TLR4) Signaling, J. Med. Chem.

(2017). https://doi.org/10.1021/acs.jmedchem.7b00095.

[37] A. Kumar, M. Mahajan, B. Awasthi, A. Tandon, M.K. Harioudh, S. Shree, P. Singh, P.K. Shukla, R. Ramachandran, K. Mitra, S. Bhattacharjya, J.K. Ghosh, Piscidin-1-analogs with double L- and D-lysine residues exhibited different conformations in lipopolysaccharide but comparable anti-endotoxin activities, Sci. Rep. (2017). https://doi.org/10.1038/srep39925.

[38] Z.Y. Ong, S.J. Gao, Y.Y. Yang, Short synthetic β-sheet forming peptide amphiphiles as broad spectrum antimicrobials with antibiofilm and endotoxin neutralizing capabilities, Adv. Funct. Mater. 23 (2013) 3682–3692. https://doi.org/10.1002/adfm.201202850.

[39] R.F. Maldonado, I. Sá-Correia, M.A. Valvano, Lipopolysaccharide modification in gram-negative bacteria during chronic infection, FEMS Microbiol. Rev. (2016). https://doi.org/10.1093/femsre/fuw007.

[40] C. Montis, V. Generini, G. Boccalini, P. Bergese, D. Bani, D. Berti, Model lipid bilayers mimic non-specific interactions of gold nanoparticles with macrophage plasma membranes, J. Colloid Interface Sci. 516 (2018) 284–294. https://doi.org/10.1016/j.jcis.2018.01.064.

[41] C. Montis, Y. Gerelli, G. Fragneto, T. Nylander, P. Baglioni, D. Berti, Nucleolipid bilayers: A quartz crystal microbalance and neutron reflectometry study, Colloids Surfaces B Biointerfaces. 137 (2016) 203–213. https://doi.org/10.1016/j.colsurfb.2015.07.039.

[42] M. Baglioni, C. Montis, D. Chelazzi, R. Giorgi, D. Berti, P. Baglioni, Polymer Film Dewetting by Water/Surfactant/Good-Solvent Mixtures: A Mechanistic Insight and Its Implications for the Conservation of Cultural Heritage, Angew. Chemie - Int. Ed. (2018). https://doi.org/10.1002/anie.201710930.

[43] M. Mayer, T.L. James, NMR-Based Characterization of Phenothiazines as a RNA Binding Scaffoldt, J. Am. Chem. Soc. (2004). https://doi.org/10.1021/ja0398870.

[44] N.S. Bryan, M.B. Grisham, Methods to detect nitric oxide and its metabolites in biological samples, Free Radic. Biol. Med. (2007). https://doi.org/10.1016/j.freeradbiomed.2007.04.026.